

# Observation of a metal-to-insulator transition with both Mott-Hubbard and Slater characteristics in $\text{Sr}_2\text{IrO}_4$ from time-resolved photocarrier dynamics

D. Hsieh,<sup>1</sup> F. Mahmood,<sup>1</sup> D. H. Torchinsky,<sup>1</sup> G. Cao,<sup>2,3</sup> and N. Gedik<sup>1</sup><sup>1</sup>*Department of Physics, Massachusetts Institute of Technology, Cambridge, Massachusetts 02139, USA*<sup>2</sup>*Center for Advanced Materials, University of Kentucky, Lexington, Kentucky 40506, USA*<sup>3</sup>*Department of Physics and Astronomy, University of Kentucky, Lexington, Kentucky 40506, USA*

(Received 20 March 2012; published 18 July 2012)

We perform a time-resolved optical study of  $\text{Sr}_2\text{IrO}_4$  to understand the influence of magnetic ordering on the low energy electronic structure of a strongly spin-orbit coupled  $J_{\text{eff}} = 1/2$  Mott insulator. By studying the recovery dynamics of photoexcited carriers, we find that upon cooling through the Néel temperature  $T_N$  the system evolves continuously from a metal-like phase with fast ( $\sim 50$  fs) and excitation density independent relaxation dynamics to a gapped phase characterized by slower ( $\sim 500$  fs) excitation density-dependent bimolecular recombination dynamics, which is a hallmark of a Slater-type metal-to-insulator transition. However our data indicate that the high energy reflectivity associated with optical transitions into the unoccupied  $J_{\text{eff}} = 1/2$  band undergoes the sharpest upturn at  $T_N$ , which is consistent with a Mott-Hubbard type metal-to-insulator transition involving spectral weight transfer into an upper Hubbard band. These findings show  $\text{Sr}_2\text{IrO}_4$  to be a unique system in which Slater- and Mott-Hubbard-type behaviors coexist and naturally explain the absence of anomalies at  $T_N$  in transport and thermodynamic measurements.

DOI: [10.1103/PhysRevB.86.035128](https://doi.org/10.1103/PhysRevB.86.035128)

PACS number(s): 71.27.+a, 71.70.Ej, 78.47.-p

## I. INTRODUCTION

Iridium oxides are unique  $5d$  electronic systems in which spin-orbit coupling, electronic bandwidth ( $W$ ), and on-site Coulomb interactions ( $U$ ) occur on comparable energy scales. Their interplay can stabilize a novel  $J_{\text{eff}} = 1/2$  Mott insulating state in which a correlation gap is opened by only moderate Coulomb interactions owing to a spin-orbit coupling induced band narrowing.<sup>1</sup> Depending on the underlying lattice, this insulating state is predicted to realize a variety of exotic quantum phases including antiferromagnetic  $J_{\text{eff}} = 1/2$  Mott insulators on the perovskite lattice,<sup>1–3</sup> correlated topological insulators and semimetals on the pyrochlore lattice,<sup>4,6</sup> and topological spin liquids on the hyper-kagome<sup>7</sup> and honeycomb lattices.<sup>8</sup> Even more tantalizing possibilities are predicted to occur upon chemically doping these systems, ranging from high- $T_c$  superconductivity<sup>9,10</sup> to spin-triplet superconductivity.<sup>8</sup>

Intensive research has been conducted on the layered perovskite iridate  $\text{Sr}_2\text{IrO}_4$  owing to its structural and electronic similarities to undoped high- $T_c$  cuprates such as  $\text{La}_2\text{CuO}_4$ .<sup>1,9</sup> The ground-state electronic structure of  $\text{Sr}_2\text{IrO}_4$  consists of a completely filled band with total angular momentum  $J_{\text{eff}} = 3/2$  and a narrow half-filled  $J_{\text{eff}} = 1/2$  band near the Fermi level  $E_F$ .<sup>1,11,12</sup> The latter is split into an upper Hubbard band (UHB) and lower Hubbard band (LHB) due to on-site Coulomb interactions and exhibits antiferromagnetic ordering of the effective  $J_{\text{eff}} = 1/2$  moments below a Néel temperature  $T_N = 240$  K<sup>3</sup> analogous to  $\text{La}_2\text{CuO}_4$ . Although this insulating ground state has been established by angle-resolved photoemission spectroscopy<sup>1</sup> and resonant x-ray scattering<sup>11</sup> measurements, whether  $\text{Sr}_2\text{IrO}_4$  is a Mott-type ( $U \gg W$ ) insulating phase typical of  $3d$  transition metal oxides or a Slater-type ( $U \approx W$ ) insulating phase is experimentally unknown and remains a topic of active theoretical debate.<sup>10,13,14</sup> Whereas a Mott-Hubbard-type metal-to-insulator transition (MIT) is discontinuous and occurs at temperatures greater or equal to  $T_N$ , a Slater-type MIT is continuous and occurs

exactly at  $T_N$ .<sup>15</sup> Therefore the relevant experimental question is whether heating above  $T_N$  brings  $\text{Sr}_2\text{IrO}_4$  into a paramagnetic insulating phase or into a paramagnetic metallic phase and what the order of the MIT is.

Owing to an absence of clear anomalies at  $T_N$  in transport,<sup>3,16–18</sup> thermodynamic,<sup>17</sup> and optical conductivity data,<sup>19</sup> there have been conflicting interpretations about how the insulating gap behaves across  $T_N$ . In this article we use time-resolved optical spectroscopy, which is highly sensitive to the existence of energy gaps,<sup>20,21</sup> to study the temperature evolution of the electronic structure of  $\text{Sr}_2\text{IrO}_4$ . Taking advantage of qualitatively distinct relaxation dynamics of photoexcited carriers exhibited by gapped and gapless systems, we find a clear change in the ultrafast dynamics across  $T_N$  indicating a gap opening concomitant with antiferromagnetic order. Analysis of the long-time relaxation dynamics further reveals behavior that is consistent with in-gap spectral weight being continuously transferred to high energies through  $T_N$ , supporting a phase transition from low-temperature insulator to high-temperature paramagnetic metal with both Mott-Hubbard and Slater-type characteristics.

## II. EXPERIMENTAL DETAILS

In our experiment we used a Ti:sapphire oscillator producing laser pulses with center wavelength 795 nm ( $h\nu = 1.56$  eV) and near 80 fs duration. The fluence of the pump pulse, which excites electrons across the insulating gap from the occupied  $J_{\text{eff}} = 3/2$  and  $J_{\text{eff}} = 1/2$  bands to the unoccupied  $J_{\text{eff}} = 1/2$  band [inset Fig. 1(a)], was varied with neutral density filters to tune the photoexcited carrier density while the probe fluence was maintained at  $4 \mu\text{J}/\text{cm}^2$ . Both beams were focused to a  $70\text{-}\mu\text{m}$  full width at half maximum (FWHM) spot on the (001) cleaved face of the sample. The 80-MHz repetition rate was reduced to 1.6 MHz with a pulse picker to eliminate steady-state heating of the sample. Use of a

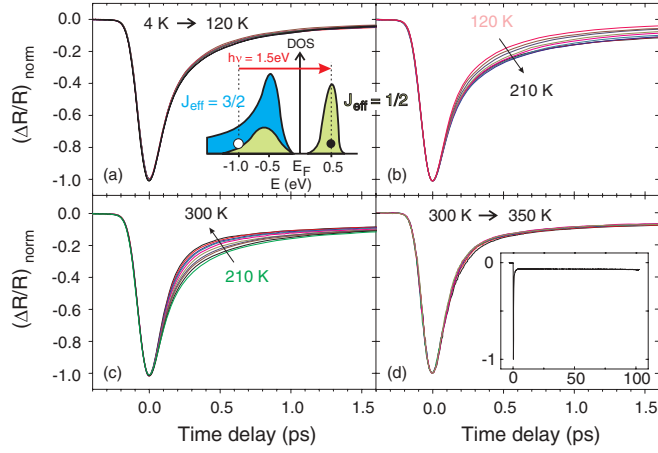


FIG. 1. (Color) Normalized time-resolved reflectivity traces  $(\Delta R/R)_{\text{norm}}$  of  $\text{Sr}_2\text{IrO}_4$  collected in the temperature ranges (a) 4–120 K, (b) 120–210 K, (c) 210–300 K, and (d) 300–350 K. Curves are collected in 10-K intervals with a pump fluence of  $15.4 \mu\text{J}/\text{cm}^2$ . Inset of panel (a) shows a schematic of the low-energy electronic density of states (DOS) based on calculations.<sup>12</sup> The red arrow denotes the optical transition being excited by the pump pulse. Inset of panel (d) shows the  $T = 300$  K trace out to 100-ps time delay.

double-modulation scheme<sup>20</sup> provided sensitivity to the fractional change of reflectivity on the order  $\Delta R/R \sim 10^{-7}$ . Single crystals of  $\text{Sr}_2\text{IrO}_4$  were grown using a self-flux technique and magnetization measurements show a magnetic ordering temperature at  $T_N = 240$  K.<sup>3,17</sup>

### III. RESULTS AND ANALYSIS

Figure 1 shows typical time-resolved reflectivity transients measured over a range of temperatures spanning 4–350 K, which have all been normalized to their negative peak values in order to emphasize the recovery dynamics. We note that the temperature here refers to that before the pump excitation, which will be lower than the instantaneous electronic temperatures reached in the ps time windows following photoexcitation. Following the pump excitation, the electronic temperature is elevated above the initial equilibrium temperature and all  $\Delta R/R$  traces exhibit a rapid negative spike, which indicates a decrease in reflectivity. Within approximately 1 ps, the reflectivity recovers to a small negative offset that persists beyond 100 ps [Fig. 1(d) inset]. By performing a temperature dependence study we find that the initial  $\sim 1$ -ps recovery can actually be decomposed into two separate components as follows. Figure 1(a) shows that between 4 and 120 K there is no discernible change in the recovery dynamics. Upon heating from 120 to 210 K [Fig. 1(b)], we find no temperature dependence within the first  $\sim 100$  fs but observe a clear slowing down of recovery dynamics after this time. Further heating of the sample from 210 to 300 K again causes no change in the first recovery component but causes the second component to become faster [Fig. 1(c)]. All temperature dependence then completely shuts off above 300 K [Fig. 1(d)]. To understand the physical processes underlying these trends, we perform detailed fits to the  $\Delta R/R$  traces.

We fit the un-normalized time-resolved reflectivity transients  $[\Delta R/R](t)$  at all temperatures to a convolution

$[f \otimes g](t) \equiv \int_{-\infty}^{\infty} f(\xi)g(t - \xi)d\xi$  of a bi-exponential decay function  $f(t)$  and a Gaussian instrument resolution function  $g(t)$  where

$$f(t) = \begin{cases} 0; & \text{if } t < 0 \\ Ae^{-t/\tau_1} + Be^{-t/\tau_2} + C; & \text{if } t > 0, \end{cases}$$

and

$$g(t) = \frac{1}{\sigma\sqrt{2\pi}} e^{-t^2/2\sigma^2},$$

where  $\sigma$  is experimentally determined by measuring an autocorrelation of our laser pulses.

To demonstrate that the  $[\Delta R/R](t)$  traces are described by a minimum of two exponential decays, we fit  $[f \otimes g](t)$  to our data at positive time delays to both a single and double exponential decay. We show fits to the data in two extreme cases: (i) data taken at a temperature  $T = 300$  K and pump fluence  $F = 15.4 \mu\text{J}/\text{cm}^2$ , where the magnitude of the slower decay component is shown to be smallest [shown later in Fig. 4(c)], (ii) data taken at a temperature  $T = 180$  K and pump fluence  $F = 1.9 \mu\text{J}/\text{cm}^2$ , where the magnitude of the slower decay component is shown to be largest [shown later in Fig. 4(c)]. Figure 2 shows that in both extremes, the data can only be satisfactorily described by two exponential decays. A decomposition of the fits into its individual components (Fig. 2) shows that the slow component is required to account for the curvature in  $\Delta R/R$  around 0.5 ps. The fitted parameters listed in red show that their standard error is small, less than the size of the symbols plotted in all the figures. We found that the fit results are not sensitive to changes of order  $\pm 40\%$  in their initial estimated values.

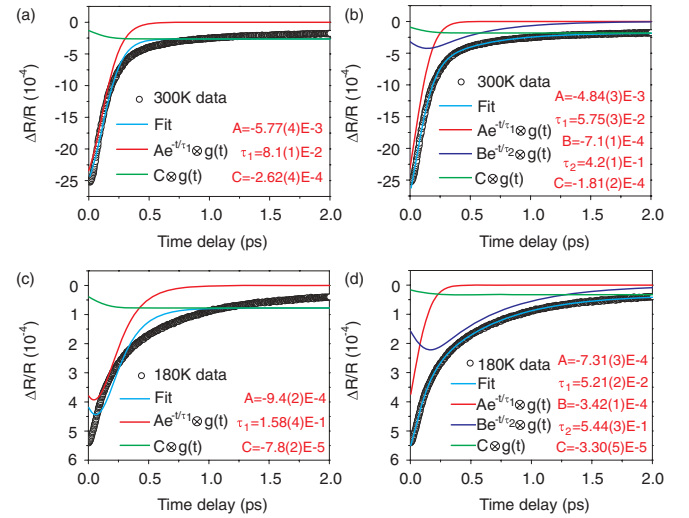


FIG. 2. (Color) Transient reflectivity traces taken at  $T = 300$  K and  $F = 15.4 \mu\text{J}/\text{cm}^2$  and fitted to a (a) single and (b) double exponential decay. Transient reflectivity traces taken at  $T = 180$  K and  $F = 1.9 \mu\text{J}/\text{cm}^2$  and fitted to a (c) single and (d) double exponential decay. Curves show the overall fit as well as the separate components of the fit. The fitted parameters and their associated fitting errors (in parentheses) are listed in red.

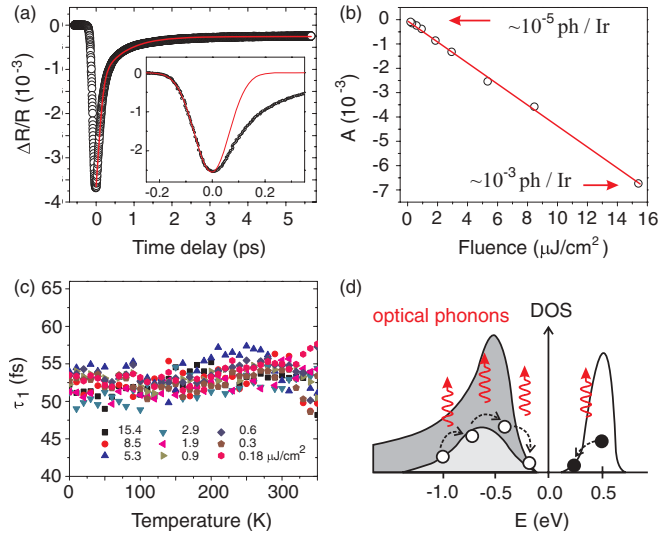


FIG. 3. (Color) (a) A typical un-normalized time-resolved reflectivity transient ( $\Delta R/R$ ) of  $\text{Sr}_2\text{IrO}_4$  overlaid with a bi-exponential fit described in the text (red curve). Inset shows the Gaussian instrument time resolution (red curve) superimposed on 300-K data where decay dynamics are dominated by the fast ( $\tau_1$ ) component [Fig. 4(b)]. This shows that the fast initial decay is not resolution limited. (b) The fitted amplitude ( $A$ ) of the fast exponential decay component measured over a range of pump fluences corresponding to  $\sim 10^{-5}$  to  $\sim 10^{-3}$  pump photons per iridium atom. The red line is a linear fit. (c) Temperature dependence of the fitted decay time ( $\tau_1$ ) of the fast exponential decay component measured over a range of pump fluences. (d) Schematic showing that the initial fast decay process is governed by energy relaxation of photoexcited electrons and holes towards the band edges via optical phonon emission. The errors in the fit parameters are smaller than the size of the symbols.

### A. Fast decay component

We begin by trying to understand the physical origin of the first decay component, which is resolved by our ultrashort laser pulses [Fig. 3(a)]. To investigate whether this fast decay arises from thermalization of photoexcited carriers via carrier-carrier scattering, whose rate should depend on the number of photoexcited carriers,<sup>22</sup> we measured  $\tau_1$  over a range of pump fluences spanning a photoexcitation density  $d$  between  $\sim 10^{-5}$  to  $\sim 10^{-3}$  photons per iridium site. We estimate  $d$  using the expression  $d = \frac{N}{n\sigma\xi}$ , where  $N$  is the number of photons per pump pulse,  $n$  is the number of iridium sites per unit volume,  $\sigma$  is the area of the sample illuminated by the pump pulse, and  $\xi$  is the optical penetration depth of photons with wavelength  $\lambda = 795$  nm. The penetration depth  $\xi$  is derived through the Beer-Lambert law  $\xi = \frac{\lambda}{4\pi k}$ .<sup>23</sup> The extinction coefficient  $k$ , equal to the imaginary part of the index of refraction, can be calculated using Eq. (8) in Ref. 24 from the amplitude ( $R$ ) and phase ( $\phi$ ) of the reflection coefficient of  $\text{Sr}_2\text{IrO}_4$ . We use available published values of  $R$  and  $\phi$  from lightly Rh-doped  $\text{Sr}_2\text{IrO}_4$  thin films,<sup>25</sup> whose optical conductivity spectrum is nearly identical to bulk single crystalline  $\text{Sr}_2\text{IrO}_4$ .

A linear behavior of the component amplitude ( $A$ ) over this fluence range [Fig. 3(b)] shows that the number of photoexcited carriers is indeed proportional to the pump fluence. Figure 3(c) shows that  $\tau_1 \approx 50$  fs exhibits no discernible fluence nor temperature dependence between 4 and 350 K.

This implies that the initial decay is not caused by photocarrier thermalization but more likely by photocarrier cooling, and that this cooling is not mediated by thermally occupied phonons. The participation of magnons is also negligible because  $\tau_1$  is insensitive to  $T_N$ . Given that the fast time scale of  $\tau_1$  is consistent with typical optical phonon-mediated cooling processes and that the Debye temperature of  $\text{Sr}_2\text{IrO}_4$ <sup>16</sup> far exceeds our measurement temperatures, we conclude that the initial fast recovery of  $\Delta R/R$  is due to the cooling of photoexcited carriers via generation of hot optical phonons [Fig. 3(d)].

### B. Slow decay component

The initial fast recovery of  $\Delta R/R$  is followed by a second slower decay component, whose amplitude ( $B$ ) exhibits an upturn upon cooling the starting equilibrium temperature of the system through  $T_N$  and then ceases to grow further below a temperature  $T_G = 175$  K [Fig. 4(a)]. The amplitude of the fast component ( $A$ ) shows comparatively little temperature dependence [Fig. 4(a)], therefore the temperature dependence of their relative amplitude ( $B/A$ ) is dominated by the features observed in  $B$  [Figs. 4(b) and 4(c)]. This indicates that at temperatures far above  $T_N$  the electronic energy relaxation occurs predominantly through the lone process of optical phonon generation described in Fig. 3 and that a separate relaxation mechanism grows near  $T_N$  before saturating below  $T_G$ . The decay time  $\tau_2$  shows a similar upturn upon cooling through  $T_N$  from around 0.36 ps at 350 K to 0.55 ps at  $T_G$  and then exhibits a marked change in temperature dependence below  $T_G$  [Fig. 4(d)]. A sharp rise in relaxation time at  $T_N$  typically signifies the development of an energy gap,<sup>20,21</sup> where a depletion of states around  $E_F$  greatly reduces the efficiency of photocarrier relaxation from above to below  $E_F$ .

The hallmark of a fully formed energy gap is that photoexcited occupied states above  $E_F$  and empty states below  $E_F$  can only combine in a pairwise fashion. Therefore, unlike in a metal, the recombination rate should be proportional to the density of photoexcited electron-hole pairs.<sup>26</sup> We find that a clear fluence dependence of  $\tau_2$  develops only below  $T_G$  [Fig. 4(d)] and that the low-temperature relaxation rate  $\tau_2^{-1}$  indeed increases linearly with fluence below  $5 \mu\text{J}/\text{cm}^2$  [Fig. 4(e)]. This shows that below  $T_G$ ,  $\tau_2$  represents the time scale for recombination of photoexcited electron-hole pairs across the insulating gap, which in the Mott-Hubbard limit corresponds to the recombination of empty and doubly occupied sites [inset Fig. 4(e)]. This ultrafast sub-ps recombination time in  $\text{Sr}_2\text{IrO}_4$  is comparable to that observed in the two-dimensional (2D) antiferromagnetic cuprate Mott insulators,<sup>27</sup> which has been attributed to additional recombination channels involving hot magnon generation. Altogether these observations allow us to conclude that at temperatures far above  $T_N$  the system behaves like a metal. Near  $T_N$  the density of states around  $E_F$  is continually depleted upon cooling, which is consistent with optical conductivity measurements,<sup>19</sup> and the insulating gap is fully developed below  $T_G$ .

To rule out the possibility that the observed temperature-dependent features are artifacts of cross correlation between our five fitting parameters, we note that based on Figs. 3(c) and 4(a) the parameters  $A$  and  $\tau_1$  exhibit no pronounced features at the temperatures of interest  $T_N$  and  $T_G$ . Moreover, we show



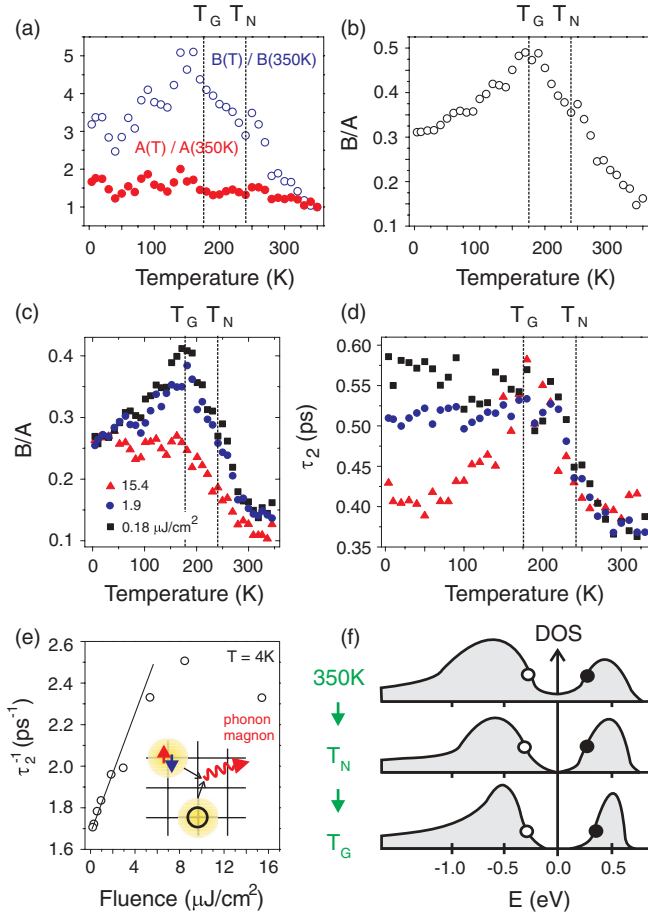


FIG. 4. (Color) (a) Temperature dependence of the fit parameters  $A$  and  $B$ , normalized to their values at  $T = 350$  K, taken in the low pump fluence regime. (b) Temperature dependence of  $B/A$  derived from data shown in (a). (c) Temperature dependence of the amplitude ratio and (d) the decay time of the slower component ( $\tau_2$ ) measured using three different fluences 15.4  $\mu\text{J}/\text{cm}^2$ , 1.9  $\mu\text{J}/\text{cm}^2$ , and 0.18  $\mu\text{J}/\text{cm}^2$ . (e) Fluence dependence of the slower decay rate measured at 4 K. Straight line is a guide to the eye showing a linear dependence at low fluences. The errors in the fit parameters are less than the size of the symbols. A schematic of the bimolecular relaxation process involving the annihilation of photoexcited empty and doubly occupied sites via emission of optical phonons or magnons is shown in the inset, which emphasizes the Mott-Hubbard character of the system. (f) Schematic showing the temperature evolution of the low-energy electronic density of states (DOS) in  $\text{Sr}_2\text{IrO}_4$  based on our data. Filled and empty circles denote the photoexcited electron and hole respectively.

in the following section that the feature at  $T_N$  observed in the temperature dependence of  $C$  is completely independent of the fitted parameters associated with the two exponential decays. Therefore the only parameters that show features at  $T_N$  and  $T_G$  and may be interdependent are  $B$  and  $\tau_2$ . However, the fitting errors associated with  $B$  and  $\tau_2$  are very small (Fig. 2), which is further support that their temperature dependence is real and robust.

The occurrence of the metal-to-insulator transition at  $T_N$  in  $\text{Sr}_2\text{IrO}_4$  (Fig. 4) distinguishes it from archetypal Mott insulators such as  $\text{MnO}$  where the insulating gap persists even in the absence of long-range magnetic order.<sup>28</sup> The

continuous nature of the MIT and its development over a broad ( $0.7 \lesssim T/T_N \lesssim 1.4$ ) temperature window further precludes a Mott-Hubbard description, which predicts sharp first-order MITs like in  $\text{V}_2\text{O}_3$ .<sup>28</sup> Although our measurements do not rule out gaps beginning to form in microscopically segregated regions above a bulk MIT temperature ( $T_{\text{MIT}}$ ), such as the case in doped  $\text{V}_2\text{O}_3$ ,<sup>29</sup> the fact that such gap opening takes place exactly across  $T_N$  in  $\text{Sr}_2\text{IrO}_4$  defies a strict Mott-Hubbard description. We rule out the possibility of a disorder broadened  $T_{\text{MIT}}$  in our samples based on their sharp magnetic susceptibility curves.<sup>3,17</sup> Although these results point towards a second-order Slater-type MIT,  $\text{Sr}_2\text{IrO}_4$  does not conform to a weakly correlated ( $U \ll W$ ) spin-density wave description, which are driven purely by Fermi surface nesting and are typically only partially gapped below  $T_N$ . Unlike a conventional spin-density wave system, magnetic ordering in  $\text{Sr}_2\text{IrO}_4$  does not change the size of the unit cell<sup>11</sup> and local moment fluctuations exist well above  $T_N$  according to both magnetic susceptibility<sup>3,17</sup> and magnetic diffuse x-ray scattering measurements.<sup>30</sup> While these magnetic signatures provide evidence for correlation physics at play, a direct electronic distinction between a correlation driven MIT and a Fermi surface nesting driven MIT is whether or not, respectively, spectral weight is transferred from low (near  $E_F$ ) energies to high (of order  $U$ ) energies upon traversing the MIT.<sup>31</sup>

### C. Offset component

To determine whether the in-gap spectral weight lost at  $T_N$  is being transferred to upper and lower Hubbard bands, we investigate the temperature dependence of the optical reflectivity at the energy scale of optical transitions from the occupied  $J_{\text{eff}} = 1/2$  and  $J_{\text{eff}} = 3/2$  bands to the unoccupied  $J_{\text{eff}} = 1/2$  band [inset Fig. 1(a)] by studying the small negative offset term  $C$  in the un-normalized  $\Delta R/R$  traces. The two exponential relaxation processes have been identified as intraband cooling and recombination processes that both lead to a transfer of energy from the electronic to lattice subsystems, which brings them into thermal equilibrium within the first few ps [Fig. 5(a)]. Subsequent cooling of this heated sample spot back to the initial temperature takes place through the diffusion

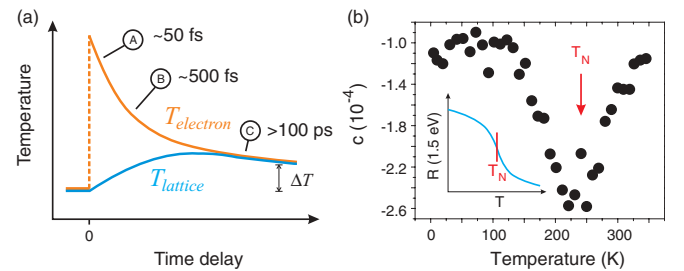


FIG. 5. (Color) (a) Diagram illustrating the temporal equilibration between the electronic and lattice subsystems following a pump pulse. The slowest process (C) is the cooling of the equilibrated system via diffusion of hot carriers or hot phonons away from the measured sample spot. (b) Temperature dependence of the offset ( $C$ ) measured using a pump fluence of 15.4  $\mu\text{J}/\text{cm}^2$ . A clear minimum in  $C$  is observed at  $T_N$  corresponding to a rapid rise in reflectivity at 1.5 eV at  $T_N$  (see inset schematic). The errors in the fit parameters are less than the size of the symbols.

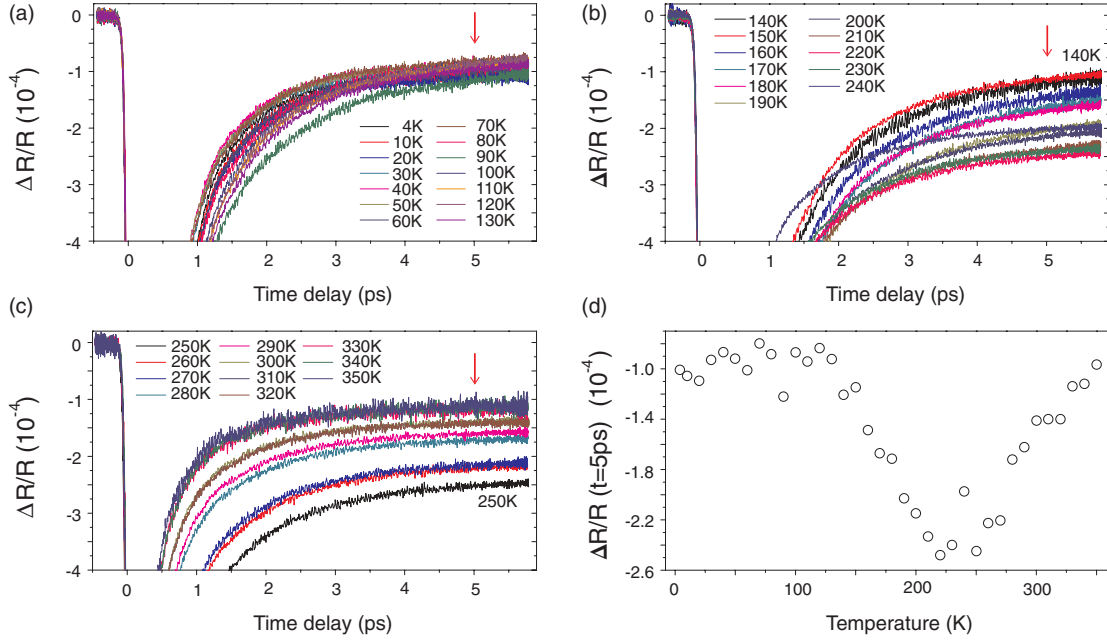


FIG. 6. (Color) Temperature dependence of un-normalized  $\Delta R/R$  traces that are plotted over a range to emphasize the long time offset. Data are plotted from (a)  $T = 4$ –130 K, (b) 140–240 K, and (c) 250–350 K in increments of 10 K. (d) The value of  $\Delta R/R$  at a time delay of 5 ps [red arrows in panels (a)–(c)] plotted as a function of temperature.

of hot carriers or hot phonons away from the laser illuminated area, which is estimated to well exceed 100 ps based on thermal conductivity and heat capacity data for  $\text{Sr}_2\text{IrO}_4$ .<sup>16</sup> To estimate the time required for heat to escape the laser excited region of the  $\text{Sr}_2\text{IrO}_4$  crystal, we calculate its thermal diffusivity  $D_{\text{th}} = \frac{k}{\rho c}$  where  $k$  is the thermal conductivity,  $\rho$  is the density, and  $c$  is the specific heat. We use the values measured at  $T = 100$  K in Ref. 16 of  $k = 2.5$  W/m K,  $\rho = 7440$  kg/m<sup>3</sup>, and  $c = 30$  J/kg K, which yields  $D_{\text{th}} = 1.1 \times 10^{-5}$  m<sup>2</sup>/s. From this we estimate the time needed for heat to diffuse out of a  $1\text{-}\mu\text{m}^2$  area to be around 1 ns. Therefore to a very good approximation the offset  $C$  is a measure of the fractional change in reflectivity at 1.5 eV due to a small temperature change  $\Delta T$  [Fig. 5(a)], namely  $C = \frac{R(T+\Delta T) - R(T)}{R(T)}$ . We estimate that at high pump fluences  $\Delta T$  is of order 1 K because  $C$  is of order  $10^{-4}$  and the fractional decrease in optical conductivity at 1.5 eV is estimated to be 2% from 10 to 500 K.<sup>19</sup> The ability to resolve such small temperature-induced changes in reflectivity is an advantage our nonequilibrium technique has over conventional equilibrium optical spectroscopy. Figure 5(b) shows that the temperature dependence of  $C$  exhibits a broad negative peak with an extremum exactly at  $T_N$ , which indicates that a small temperature rise causes the largest decrease of the 1.5-eV reflectivity exactly at  $T_N$ . From this we can infer a broad temperature window ( $0.6 \lesssim T/T_N \lesssim 1.4$ ) within which  $R$  (1.5 eV) starts to rise sharply with cooling, with the greatest slope occurring at  $T_N$  [inset Fig. 5(b)]. The fact that this temperature window largely coincides with that over which  $\tau_2$  increases most drastically [Fig. 4(d)] is consistent with a Mott-Hubbard mechanism where spectral weight is transferred from low in-gap energies ( $\sim 0.1$  eV<sup>12</sup>) to energies (1.5 eV) far exceeding it.

To demonstrate that this behavior is independent of our fitting procedure, we show that the temperature dependence

of the long time offset in  $\Delta R/R$ , the asymptotic value of the un-normalized reflectivity variation after the first two fast decay processes, can be obtained even without fitting. Figure 6(a) shows that between  $T = 4$  and 130 K, this asymptotic value does not show a measurable systematic variation with temperature. Upon heating from 140 to 240 K [Fig. 6(b)], the offset clearly decreases with heating and upon heating further from 250 to 350 K [Fig. 6(c)], the offset exhibits a clear increase with heating. By plotting the value of  $\Delta R/R$  at 5 ps as a function of temperature [Fig. 6(d)], we can already visualize the temperature dependence of the offset, which is very similar to that obtained through fitting [Fig. 5(b)]. This proves that the peak observed at  $T_N$  in the offset  $C$  is independent of how we fit the initial fast dynamics.

We note that variations in reflectivity can also be caused by a narrowing or shift of Lorentz oscillators representing direct optical transitions at 1.5 eV that do not involve spectral weight redistribution, and that our measurements do not distinguish between density of states changes in the occupied  $J_{\text{eff}} = 3/2$  and  $J_{\text{eff}} = 1/2$  initial states versus the unoccupied  $J_{\text{eff}} = 1/2$  final state. However, there is no current explanation for how such changes can be induced via magnetic ordering in the  $J_{\text{eff}} = 1/2$  band. Regardless, the observed temperature dependence of the quasiequilibrium reflectivity at 1.5 eV is unusual because the relaxation rate behavior suggests a Slater-type behavior (Fig. 4), which should be dominated by low-energy physics near the Fermi level and have little effect on the high-energy reflectivity.

#### IV. CONCLUSIONS

Our results taken altogether suggest that unlike  $\text{La}_2\text{CuO}_4$ , which remains a Mott insulator far above its magnetic ordering

temperature,  $\text{Sr}_2\text{IrO}_4$  undergoes a metal-to-insulator transition across  $T_N$ . This suggests that  $\text{Sr}_2\text{IrO}_4$  is more accurately described as an intermediate coupling ( $U \approx W$ ) insulator that exhibits both Mott-Hubbard and Slater-type characteristics. Our observation that this metal-to-insulator transition takes place over a wide temperature window compared to  $T_N$  naturally explains the lack of sharp anomalies at  $T_N$  in transport, thermodynamic, and optical conductivity data. We argue that these may be signatures of a rare example of a temperature-controlled continuous metal-to-insulator transition in a quasi-two-dimensional system hitherto unobserved in any  $d$ -electron material,<sup>28</sup> and may also be applicable to the wider class of  $J_{\text{eff}} = 1/2$  Mott insulating perovskite, honeycomb, hyperkagome, and pyrochlore iridates. Moreover,

transport data on  $5d$  Os oxides suggestive of continuous metal-to-insulators transitions<sup>32</sup> show that the confluence of strong spin-orbit coupling and on-site Coulomb interactions is a general playground for unconventional metal-to-insulator transitions.

## ACKNOWLEDGMENTS

We thank F. Wang, T. Senthil, A. Vishwanath, S. Kehrlein, K. Michaeli, R. Flint, S. Drapcho, and Y. Wang for useful discussions. N.G. acknowledges support from Army Research Office Grant No. W911NF-11-1-0331. C.G. acknowledges support through National Science Foundation Grants No. DMR-0856234 and No. EPS-0814194.

- <sup>1</sup>B. J. Kim *et al.*, *Phys. Rev. Lett.* **101**, 076402 (2008).
- <sup>2</sup>H. Okabe, N. Takeshita, M. Isobe, E. Takayama-Muromachi, T. Muranaka, and J. Akimitsu, *Phys. Rev. B* **84**, 115127 (2011).
- <sup>3</sup>G. Cao, J. Bolivar, S. McCall, J. E. Crow, and R. P. Guertin, *Phys. Rev. B* **57**, R11039 (1998).
- <sup>4</sup>D. Pesin and L. Balents, *Nat. Phys.* **6**, 376 (2010).
- <sup>5</sup>B.-J. Yang and Y. B. Kim, *Phys. Rev. B* **82**, 085111 (2010).
- <sup>6</sup>X. Wan, A. M. Turner, A. Vishwanath, and S. Y. Savrasov, *Phys. Rev. B* **83**, 205101 (2011).
- <sup>7</sup>M. J. Lawler, H.-Y. Kee, Y. B. Kim, and A. Vishwanath, *Phys. Rev. Lett.* **100**, 227201 (2008).
- <sup>8</sup>Y.-Z. You, I. Kimchi, and A. Vishwanath, *arXiv:1109.4155*.
- <sup>9</sup>F. Wang and T. Senthil, *Phys. Rev. Lett.* **106**, 136402 (2011).
- <sup>10</sup>C. Martins, M. Aichhorn, L. Vaugier, and S. Biermann, *Phys. Rev. Lett.* **107**, 266404 (2011).
- <sup>11</sup>B. J. Kim, H. Ohsumi, T. Komesu, S. Sakai, T. Morita, H. Takagi, and T. Arima, *Science* **323**, 1329 (2009).
- <sup>12</sup>H. Watanabe, T. Shirakawa, and S. Yunoki, *Phys. Rev. Lett.* **105**, 216410 (2010); H. Jin, H. Jeong, T. Ozaki, and J. Yu, *Phys. Rev. B* **80**, 075112 (2009).
- <sup>13</sup>R. Arita, J. Kunes, A. V. Kozhevnikov, A. G. Eguiluz, and M. Imada, *Phys. Rev. Lett.* **108**, 086403 (2012).
- <sup>14</sup>G. Jackeli and G. Khaliullin, *Phys. Rev. Lett.* **102**, 017205 (2009).
- <sup>15</sup>N. F. Mott, *Metal-Insulator Transitions* (Taylor & Francis, London, 1990); F. Gebhard, *The Mott Metal-Insulator Transition* (Springer, Berlin, 1997).
- <sup>16</sup>N. S. Kini, A. M. Strydom, H. S. Jeevan, C. Geibel, and S. Ramakrishnan, *J. Phys.: Condens. Matter* **18**, 8205 (2006).
- <sup>17</sup>S. Chikara, O. Korneta, W. P. Crummett, L. E. DeLong, P. Schlottmann, and G. Cao, *Phys. Rev. B* **80**, 140407(R) (2009).
- <sup>18</sup>M. Ge, T. F. Qi, O. B. Korneta, D. E. DeLong, P. Schlottmann, W. P. Crummett, and G. Cao, *Phys. Rev. B* **84**, 100402(R) (2011).
- <sup>19</sup>S. J. Moon, H. Jin, W. S. Choi, J. S. Lee, S. S. A. Seo, J. Yu, G. Cao, T. W. Noh, and Y. S. Lee, *Phys. Rev. B* **80**, 195110 (2009).
- <sup>20</sup>N. Gedik, P. Blake, R. C. Spitzer, J. Orenstein, R. Liang, D. A. Bonn, and W. N. Hardy, *Phys. Rev. B* **70**, 014504 (2004).
- <sup>21</sup>E. E. M. Chia, J. X. Zhu, H. J. Lee, N. Hur, N. O. Moreno, E. D. Bauer, T. Durakiewicz, R. D. Averitt, J. L. Sarrao, and A. J. Taylor, *Phys. Rev. B* **74**, 140409(R) (2006).
- <sup>22</sup>J. Hohlfeld, J. G. Müller, S.-S. Wellershoff, and E. Matthias, *Appl. Phys. B* **64**, 387 (1997).
- <sup>23</sup>I. Simon, *J. Opt. Soc. Am.* **41**, 336 (1951).
- <sup>24</sup>H. J. Bowlden and J. K. Wilmshurst, *J. Opt. Soc. Am.* **53**, 1073 (1963).
- <sup>25</sup>J. S. Lee, Y. Krockenberger, K. S. Takahashi, M. Kawasaki, and Y. Tokura, *Phys. Rev. B* **85**, 035101 (2012).
- <sup>26</sup>A. Rothwarf and B. N. Taylor, *Phys. Rev. Lett.* **19**, 27 (1967).
- <sup>27</sup>H. Okamoto, T. Miyagoe, K. Kobayashi, H. Uemura, H. Nishioka, H. Matsuzaki, A. Sawa, and Y. Tokura, *Phys. Rev. B* **83**, 125102 (2011).
- <sup>28</sup>M. Imada, A. Fujimori, and Y. Tokura, *Rev. Mod. Phys.* **70**, 1039 (1998).
- <sup>29</sup>S. Lupi *et al.*, *Nature Comm.* **1**, 105 (2010).
- <sup>30</sup>S. Fujiyama, H. Ohsumi, T. Komesu, J. Matsuno, B. J. Kim, M. Takata, T. Arima, and H. Takagi, *Phys. Rev. Lett.* **108**, 247212 (2012).
- <sup>31</sup>G. Kotliar and D. Vollhardt, *Phys. Today* **57**(3), 53 (2004).
- <sup>32</sup>D. Mandrus, J. R. Thompson, R. Gaal, L. Forro, J. C. Bryan, B. C. Chakoumakos, L. M. Woods, B. C. Sales, R. S. Fishman, and V. Keppens, *Phys. Rev. B* **63**, 195104 (2001); Y. G. Shi *et al.*, *ibid.* **80**, 161104(R) (2009).